THE ASTROPHYSICAL JOURNAL, 399:57–65, 1992 November 1

LARGE INFRARED AND OPTICAL COLOR GRADIENTS IN THE CARTWHEEL RING GALAXY: EVIDENCE FOR THE FIRST EPOCH OF STAR FORMATION IN THE WAKE OF AN EXPANDING RING

P. M. MARCUM[1] AND P. N. APPLETON[2]
Iowa State University
AND
J. L. HIGDON[3]
University of Texas
Received 1992 January 16; accepted 1992 May 6

ABSTRACT

Substantial near-infrared and optical color gradients have been observed within the disk of the classical ring galaxy A0035−324 (the "Cartwheel"). The slope of the radial $B-V$, $V-K$ color gradient coincides with starburst color evolution predictions, indicating that the *age* of the disk population is a function of radius. Observations indicate that the youngest stars are on the leading edge of the outer ring, and the stellar population grows increasingly older toward the nucleus. The radial color gradient, taken together with other evidence, strongly support the collisional picture for the formation of ring galaxies. Strong IR emission observed in the outer ring appears to be directly associated with the young star-forming regions rather than an evolved stellar population. We conclude that star formation is occurring in a mainly gaseous expanding density wave and that the Cartwheel is undergoing its first epoch of star formation since its formation.

Subject headings: galaxies: individual (A0035−324) — galaxies: photometry — galaxies: stellar content — stars: formation

1. INTRODUCTION

Ring galaxies are useful tools in the study of star formation within interacting systems. Models indicate that the ring forms when a galaxy, the "intruder," collides head-on with its larger companion galaxy, the "target" (e.g., Lynds & Toomre 1976; Theys & Spiegel 1977; Toomre 1978). The resulting disturbance in the gravitational potential of the target galaxy produces outwardly propagating density waves. A nearly symmetrical ring geometry is produced if the collision takes place along the spin axis of the target galaxy, passing through the target nucleus. It is likely that star formation will be induced along the ring's perimeter when the gas density exceeds a threshold (Appleton & Struck-Marcell 1987, hereafter ASM; Struck-Marcell & Appleton 1987, hereafter SMA). These models predict that as the expanding wave of star formation propagates outward from the nucleus, evolving stars are left behind, with regions furthest from the nucleus containing the youngest stars. Thus, a memory of the star formation history is preserved in the radial color distribution of the material between the rings (hereafter, the "inter-ring" region). The large angular size of the Cartwheel (80″ along the major axis) allows for a feasible search for these anticipated color gradients. Previous broad-band optical studies (Theys & Spiegel 1976; Spight et al. 1990; Schultz et al. 1990; Thompson & Theys 1978) of other ring systems are consistent with our general result that such ring-dominated systems are quite blue.

In § 2 we describe the method of observation, and in § 3 we present the results of our primarily infrared study. A more complete description of the optical data will be published elsewhere (Higdon 1992). In § 4 we discuss the ramifications of our observations with regard to the model predictions. In particular, we show that our data provide strong support for the collisional models of ring galaxy formation. In § 5, we suggest that a density wave is propagating outward through the mainly gaseous disk of the Cartwheel, leaving in its wake the first major generation of stars in the galactic disk. The idea that the Cartwheel is undergoing an initial epoch of disk star formation was one suggestion put forth by Fosbury & Hawarden (1977, hereafter FH), whose spectroscopic observations of the Cartwheel showed low metallicities in the H II regions of the outer ring. In § 6, the properties of the knots are discussed. Finally, the colors of the companion galaxies are presented in § 7. Throughout this paper we assume a distance to the Cartwheel ring galaxy of 89 Mpc, derived assuming a Hubble constant $H_0 = 100$ km s^{-1} Mpc^{-1}. We adopt a systematic velocity[4] for the galaxy of $V_0 = 8897 \pm 10$ km s^{-1}, as derived from H I observations (Higdon 1992). For purposes of expressing distant dependent quantities, we define a scale factor, $h = H_0/100$.

2. OBSERVATIONS AND DATA REDUCTION

2.1. *Near-Infrared Observations*

Broad-band $J(\lambda$-1.25 μm), $H(\lambda$-1.65 μm), and $K(\lambda$-2.2 μm) near-IR images were obtained using the IRCAM 2 InSb photovoltaic IR array camera on the UKIRT[5] 3.8 m telescope on the nights of 1990 October 24–25. The 62 × 58 array was configured for a resolution of 1.″24 pixel.$^{-1}$ Conditions were dark and photometric for most of both nights, with a seeing disk of

[1] Postal address: Department of Astronomy, University of Wisconsin, Madison, WI 53706.
[2] Postal address: Department of Physics and Astronomy, Iowa State University, Ames, IA 50010.
[3] Postal address: Department of Astronomy, University of Texas, Austin, TX 78712.

[4] Corrected to local group: $V_0 = V_h + 300 \sin(l^{II}) \cos(b^{II})$.
[5] The United Kingdom Infrared Telescope is operated by the Royal Observatory, Edinburgh, under the support of the Science and Engineering Research Council of the UK.

$\sim 2''$. The UKIRT standard stars HD 203856, SA 92−342, G158−27, F16, HD 84800, SA 93−317, HD 3209, and HD 225023 were used for calibration. For galaxy and sky exposures, typical integration times were 126 s using 7 co-adds, 128 s using 16 co-adds, and 120 s using 20 co-adds for J, H, and K, respectively. By using four different guiding centers, we were able to provide full coverage of the Cartwheel as well as three of its companion galaxies. Blank regions of sky $\sim 3'$–$4'$ from the source were observed after every Cartwheel observation in order to provide flat-field information.

2.2. *Optical Observations*

The optical CCD imagery (Johnson B and V filters) were obtained using the McDonald Observatory 0.76 m telescope on the nights of 1989 September 25–27. A Texas Instrument (TI No. 2) 800 × 800 array was used in the direct imaging mode at the f/13.5 focus, yielding after on-chip co-addition a usable field of view of $3'.8$ with $0''.573$ pixel^{-1}. Read-out noise was determined to be $18.9e^-$. The final images were constructed by combining three frames totaling 2700 s in B and 1800 s in V. The nights were photometric and the spatial resolution in the final images were determined to be $1''.8$ FWHM in B and $1''.6$ FWHM in V. Photometric calibration was accomplished using repeated observations of the $BVRI$ standard star field in M92 (Christian et al. 1985) over a wide range in airmass.

2.3. *Near-Infrared Data Reduction*

The standard IRCAM linearization procedure was applied to all the raw image frames to remove possible nonlinearities in the detector. The remaining data reduction was performed using the Image Reduction and Analysis Facility (IRAF) image processing software developed by Kitt Peak National Observatory. After normalizing all of the images by the exposure times and removing bad pixels caused by array flaws and cosmic ray hits, dark frames were averaged and then subtracted from both the sky and source frames. Flat fields were obtained by median-averaging sky frames taken before and after the observation of the galaxy. In some cases bright stars in the sky frames were removed before averaging. After flat-fielding and removing a constant background level from each galaxy frame, the images were corrected for atmospheric extinction using average absorption coefficients for UKIRT (C. Aspen 1990, personal communication). Finally, the individual Cartwheel images were co-added to produce a mosaic of the whole field using a median-filtering algorithm developed by one of us (P. M. M.).

Much more coverage was given to the nucleus of the Cartwheel than to the other regions (especially the companion galaxies). As a result, the rms noise varies slightly across the image. The nucleus of the Cartwheel was covered by 9, 7, and 10 frames for the J, H, and K bands, respectively, whereas the outer ring had a coverage of about five frames for any point along its perimeter. There was only one set of J, H, and K images for each companion galaxy.

The photometry was performed using the POLYPHOT package in IRAF. POLYPHOT was used to define polygons which form (1) elliptical annuli centered on the nucleus of the Cartwheel (Fig. 1*a* [Plate 1]), "wedges" in the inter-ring region (see Fig. 1*b* [Plate 2]), and (3) "filled ellipses." The purpose of the filled ellipses was to compare our results with single-beam variable-aperture studies of disk systems. A large annular region exterior to the outer ring (just beyond the 1 σ contour in the J band) was defined for the "sky." The rms errors we quote for the integrated magnitudes of the various regions take into account fluctuations in the sky and Poisson counting statistics. In general, the largest contribution to the noise in our observations was due to uncertainties in the sky background.

3. RESULTS

3.1. *Near-Infrared Morphology*

Figures 1*a*–1*c* [Plates 1–3] are gray-scale images of the Cartwheel taken in the J, H, and K bands. An enlarged and rescaled view of the inner ring is also shown. The faintest structures visible correspond to the 1.5 σ level. There are four notable features in these images: (1) a prominent "hole" behind the brightest southern portion of the outer ring, (2) little or no emission exterior to the outer ring, (3) a close correspondence between the infrared and optical outer ring knots, and (4) the lack of a broad outer ring in the K-band image (notice that the width is no greater than that of the B-band image).

Figure 1*d* [Plate 4] is the K-band image smoothed with a Gaussian to an effective HPBW of $\sim 2''.4$ in order to enhance faint, extended emission. The image clearly shows that the "hole" behind the outer ring is devoid of emission. Likewise, no emission outside of the outer ring is seen down to a surface brightness level of 21.6 mag arcsec^{-2} in the smoothed K-band image. We have carefully checked the possibility that the "hole" is a result of a mismatch between the base levels in the co-added IRCAM frames (in the K-band image, the northern edge of the hole lies close to a frame boundary). However, inspection of many individual frames at all IR bands show the same depression behind the ring. Furthermore, the northern edge of the hole does not precisely follow the boundaries of the frames; in the J and H images, the hole has a somewhat more irregular shape along its northern boundary. Therefore, the near-horizontal shape of the upper edge of the hole at K is unrelated to the frame boundaries and seems to represent a real deficiency of emission behind the strongest region of a density wave.

Figure 2 is a B and K band surface density profile across the outer ring. Similar cuts were made at several locations along the outer ring, typically averaging over a width of ~ 5–6 pixels. All of the cuts that were made demonstrated a remarkable similarity between the B and K surface density profile in the outer ring; note how closely the optical and IR follow each other even at low emission levels.

The integrated optical and IR magnitudes and colors for the Cartwheel and the three companion galaxies are presented in Table 1. The errors ($\pm 0^m.3$) in the near-IR colors for the com-

TABLE 1

NEAR-INFRARED COLORS OF THE COMPANION GALAXIES

Galaxy	J (mag)	B (mag)	$J-H$ (mag)	$H-K$ (mag)	$B-V$ (mag)	$V-K$ (mag)
Cartwheel	12.21	13.86	0.49	0.17	0.18	2.13
2[a,b]	13.7	...	0.6	0.3	...	...
3[c]	13.4	16.1	0.7	0.2	0.6	3.0
4[c]	15.6	16.5	0.4	0.4	0.1	1.6

[a] Northern-most companion galaxy, labeled "?" by Davies & Morton 1982.

[b] Located on the edge of the optical image.

[c] Companion galaxies labeled according to FH.

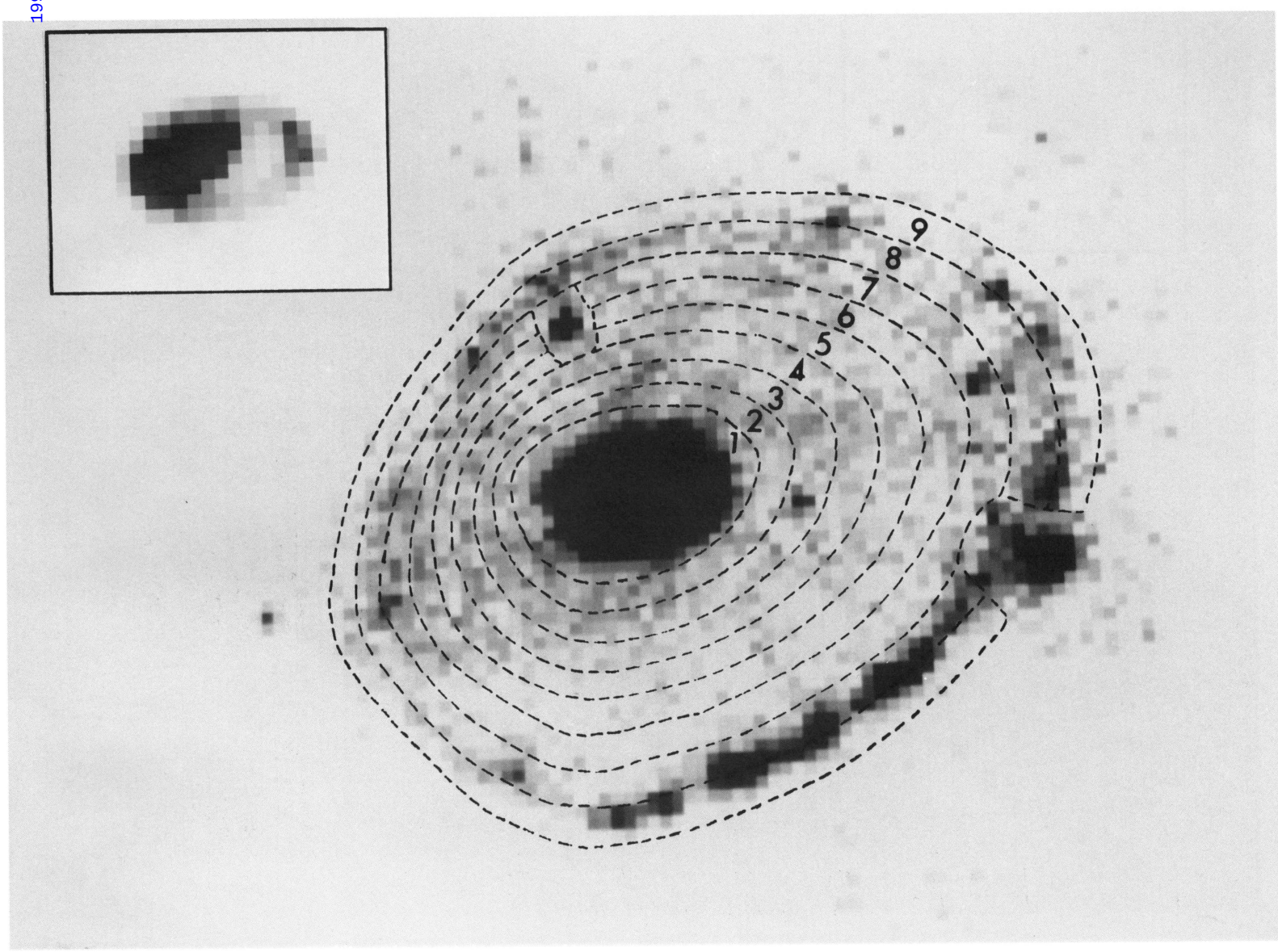

FIG. 1*a*

FIG. 1.—(*a*) Gray-scale *J* band (λ-1.25 μm) image of the Cartwheel ring galaxy. Displayed in the upper left corner is the central region which has been rescaled to show the inner ring. The numbered annuli which were used to determine radial color gradients are superimposed. The faintest features in the main image represent a 1.5 σ detection. (*b*) Same as for (*a*), but for the *H* band (λ-1.65 μm). The superposed wedges were used to determine azimuthal color gradients and surface densities. (*c*) Same as for (*a*), but for the *K* band (λ-2.20 μm). Note the strong rarefraction behind the outer ring which was predicted by ASM. Knots 6 and 9 are suspected foreground stars. (*d*) The *K*-band image, smoothed to a beam width of $\sim$2.″4 in order to emphasize faint, extended emission. Note that even after smoothing, no emission is detected in the region immediately behind the outer ring nor outside the outer ring.

PLATE 2

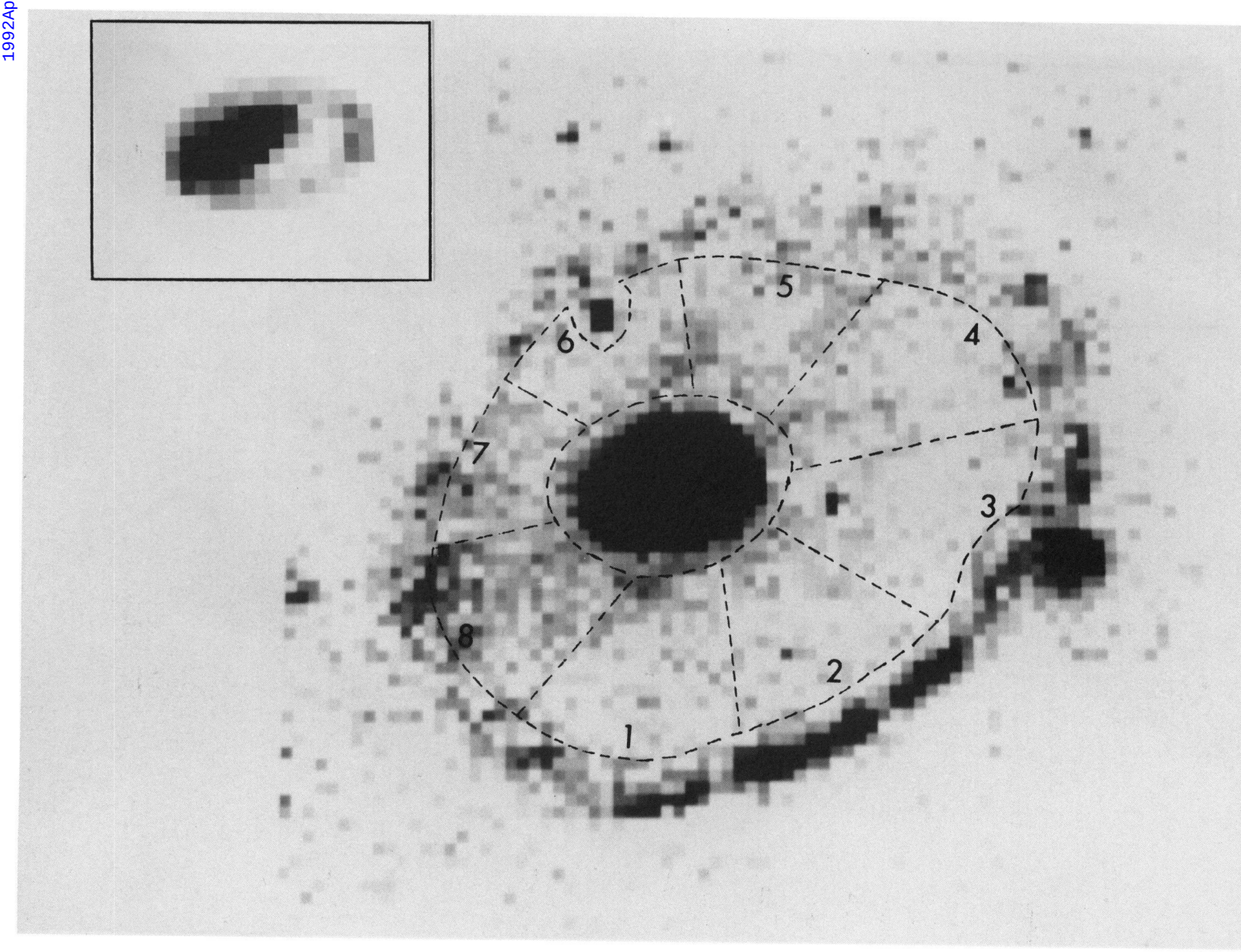

FIG. 1*b*

MARCUM, APPLETON & HIGDON (see 399, 58)

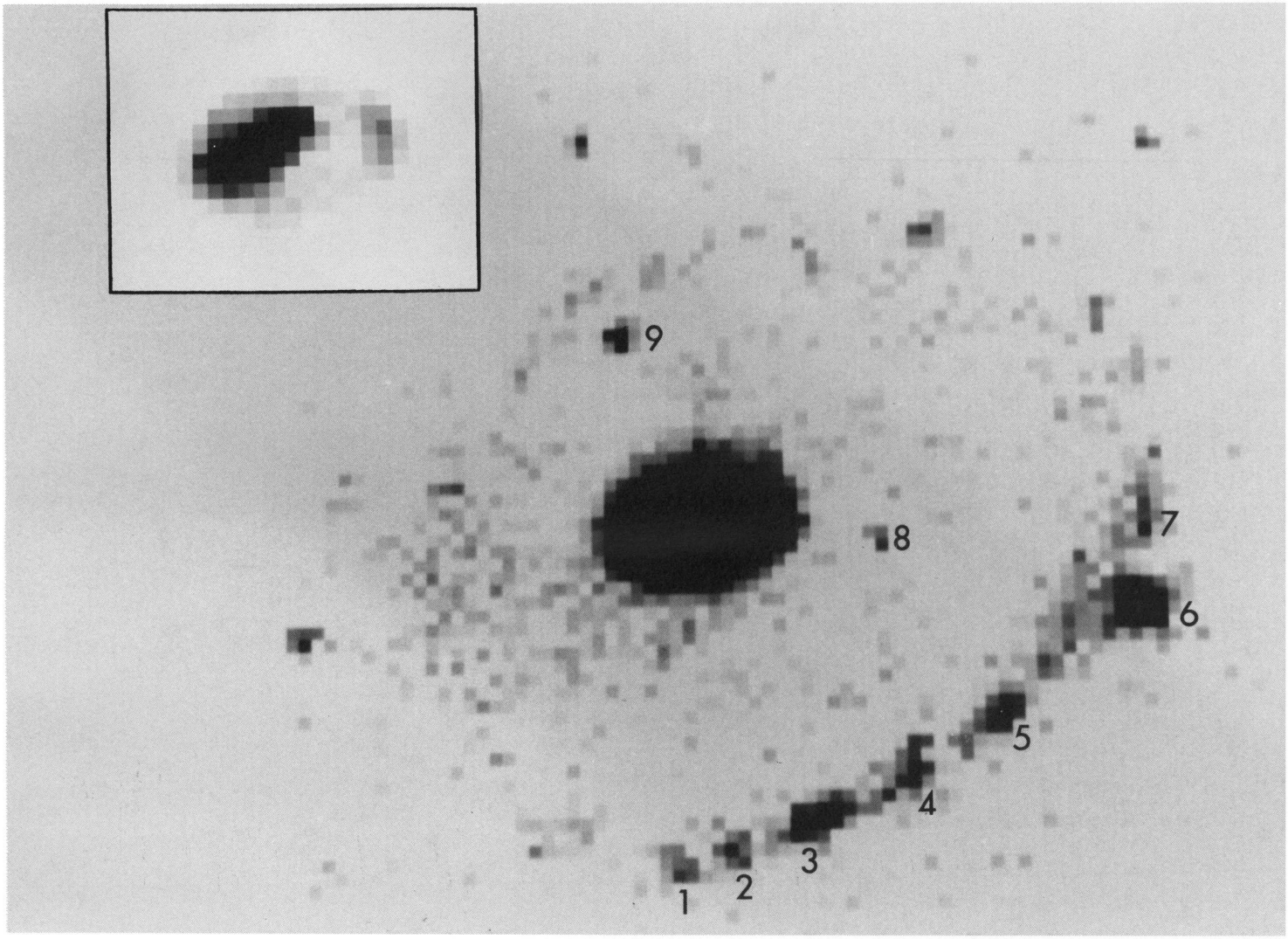

FIG. 1*c*

PLATE 4

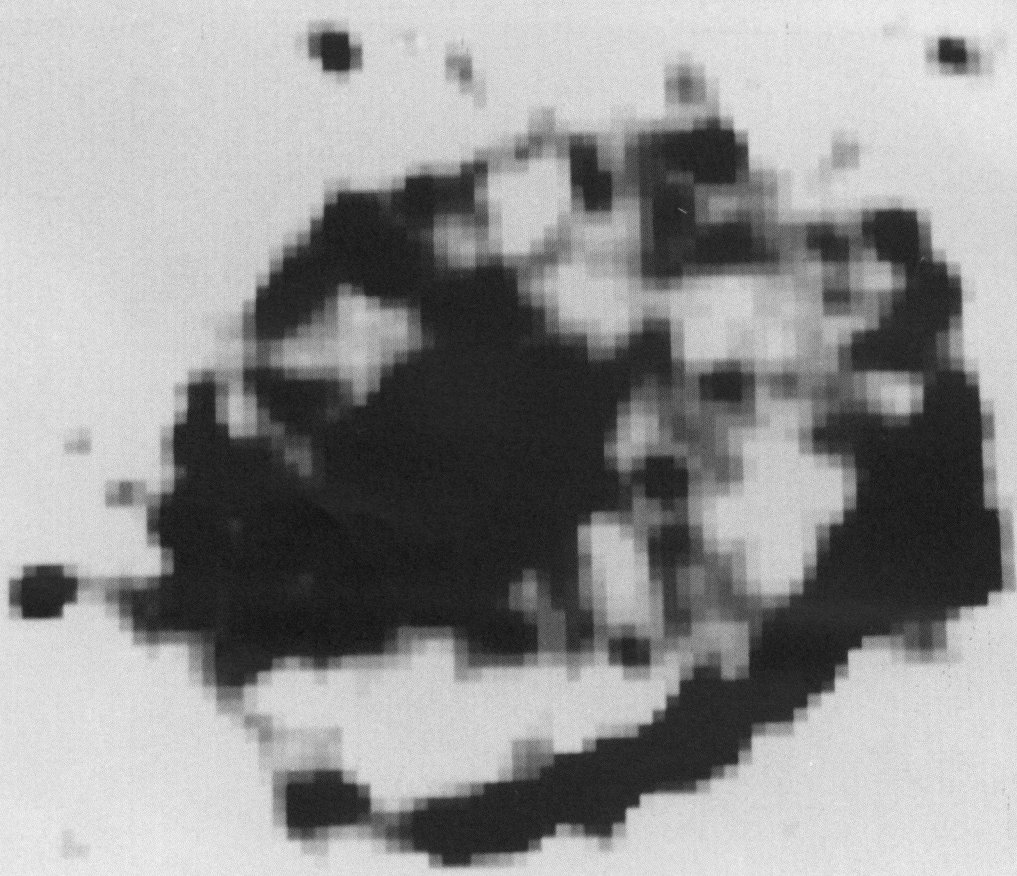

FIG. 1*d*

MARCUM, APPLETON & HIGDON (see 399, 58)

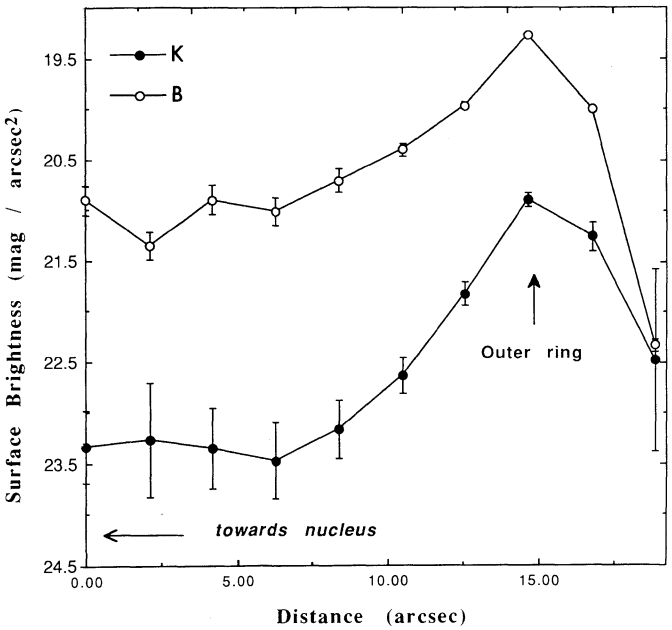

FIG. 2.—A surface brightness profile cut through the outer ring in the B and K bands, with 1 σ error bars. The distance is measured with respect to the position of the first data point, which was located approximately halfway between the inner and outer rings.

panions are significantly larger than those of the Cartwheel since much less observing time was devoted to these galaxies.

3.2. *Radial Color Gradients*

The $B-V$ and $V-K$ colors for each annular section illustrated in Figure 1*a* have been plotted in the color-color diagram of Figure 3. The annular points are numbered according to radius, beginning with the inner ring (point 1) and ending with the outer ring (points 8 and 9). The centroids of the annuli are separated by $\sim 3''$ ($= 1.29\ h^{-1}$ kpc). These data have been corrected for Galactic reddening using $A_B = 0^m.22$ (de Vaucouleurs, de Vaucouleurs, & Corwin 1976, hereafter RC2) and the standard ISM extinction curve (Bessell & Brett 1988). FH estimated the total extinction $A_v = 2^m.1$ for two of the H II regions (knots 3 and 5 in Fig. 1*c*) within the outer ring by comparing observed Balmer line intensities with those predicted by case B radiative recombination theory and assuming a standard inerstellar reddening law. Because the FH correction (see reddening vector in Fig. 3) is applicable only for the H II knots in the outer ring, the data have not been corrected for internal extinction. However, the observed color gradients are not likely to be a product of differential extinction within the disk, as no monotonic increases in the H I column density are observed in the disk (Higdon 1992).

Figure 4 illustrates the radial color gradients in $J-H$ and $H-K$ for the same annuli used in Figure 3. Internal reddening was not applied, but all of the emission regions were corrected for Galactic extinction. In the disk material lying between the inner ring (point 1) and a position midway between the two rings (point 4), the $H-K$ color *increases* continuously as one goes radially outward, while the corresponding $J-H$ color *decreases*. Proceeding outward from point 4 to the outer ring (points 8 and 9), the $H-K$ color *decreases* in $H-K$ while the $J-H$ color remains approximately constant. Note that there is a large color gradient across the outer ring itself; the outer edge of the ring (point 9) has a significantly smaller $H-K$ color than the inner edge (point 8). The effect is very noticeable in the $B-V/V-K$ diagram of Figure 3. In order to check the validity of this result we restricted our analysis to the southern quadrant of the ring (i.e., across the brightest part of the ring). We confirm that the $V-K$ color changes by $0^m.6$ over an angular scale of $6''$ ($= 3$ kpc at distance of 89 Mpc).

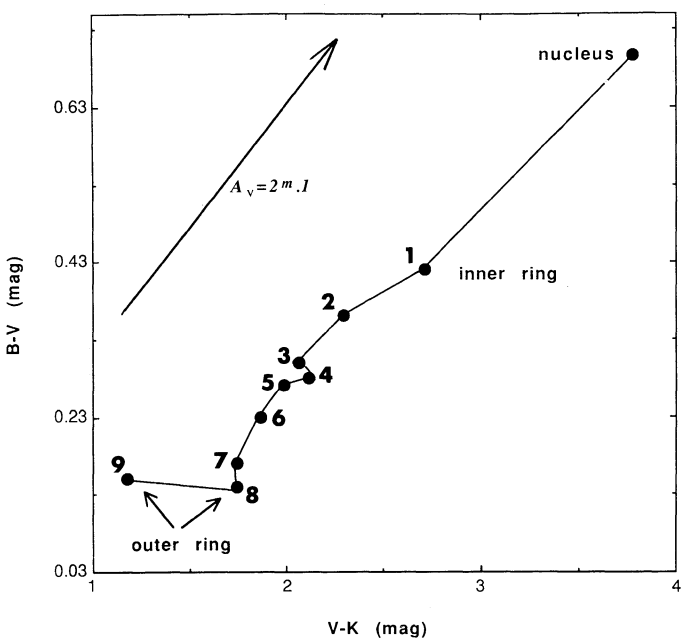

FIG. 3.—A color-color ($B-V$, $V-K$) plot for each annulus shown in Fig. 1*a*. This figure illustrates the radial dependence of the color within the disk. The data have been corrected for Galactic interstellar reddening but have not been corrected for internal extinction. The arrow indicates the effect of using $A_v = 2^m.1$, which was derived for knots 3 and 5 (FH).

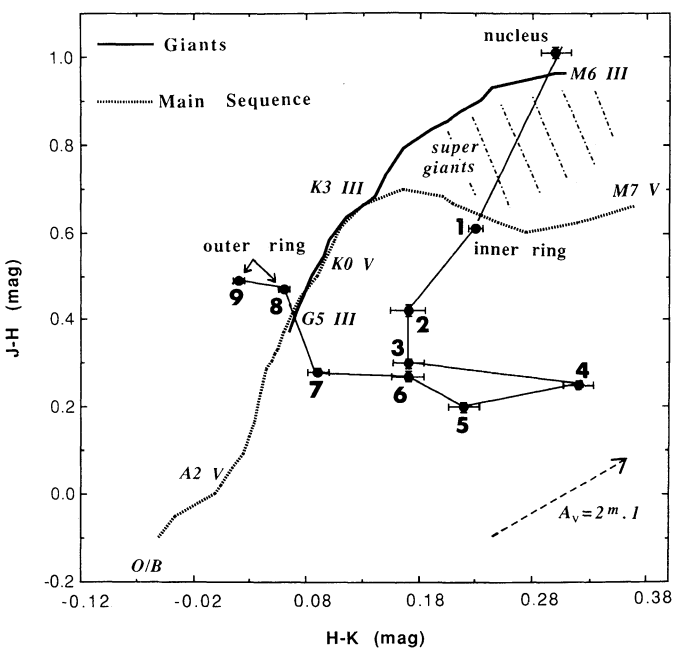

FIG. 4.—Same as for Fig. 3, but for the $J-H$, $H-K$ colors. Error bars represent a 1 σ limit. Superposed are the expected colors for a population of main-sequence, giant, and supergiant stars (Bessell & Brett 1988).

TABLE 2

RADIAL COLOR GRADIENTS[a]

COLOR	CARTWHEEL		EARLY-TYPE GALAXIES[b]
	Annular Aperture (mag)	Elliptical Aperture (mag)	Variable Aperture (mag)
$J-H$	-0.85 ± 0.03[c]	-0.41 ± 0.01	-0.033 ± 0.007
	$+1.1 \pm 0.03$		
$H-K$	-0.32 ± 0.05	-0.05 ± 0.05[d]	-0.012 ± 0.009
$B-V$	-0.5 ± 0.5	-0.5 ± 0.2	-0.15 ± 0.02
$V-K$	-2.1 ± 0.3	-1.4 ± 0.1	-0.16 ± 0.05

[a] The gradient was found by a least squares fit to a plot of color vs. log (r/R), where r/R is the fraction of the outer ring radius.

[b] Average gradients found in a survey of early-type spirals (Griersmith et al. 1982).

[c] Due to a discontinuity in the $J-H$ color, two values were given: the negative gradient is that of the inner regions, and the positive value fits the outer regions (from point 4 through point 9).

[d] The $H-K$ is rather flat for the innermost regions but falls off sharply in the outer regions. A gradient of -0.22 is obtained if the inner regions are excluded.

In addition to integrating the flux within annular regions, concentric elliptical apertures were used for comparison with radial color studies of other galaxies. Table 2 presents the radial color information and includes, for comparison, data from the study (Griersmith, Hyland, & Jones 1982) of 65 disk systems ranging from late lenticulars through Sb ($T = -1$ through 3). The later spirals in this sample would be expected to show the largest radial gradients. However, the radial color gradients within the Cartwheel as determined from the elliptical apertures exceed the average values from the Griersmith study of a factor of ~ 8. The local gradient, as determined by the annular regions, is even larger yet.

3.3. *Azimuthal Variations*

Besides radial color gradients, there are also near-IR color gradients in the azimuthal direction. The wedge-shaped apertures illustrated in Figure 1*b* were used for the azimuthal colors and surface densities. Figure 5*a* shows a $J-H/H-K$ plot of the azimuthal colors for the inter-ring region, while Figure 5*b* presents the azimuthal colors of the outer ring alone. In both diagrams, the $J-H$ color at first decreases and then increases again with increasing position angle (the position angle is measured counterclockwise with respect to wedge 1 on Fig. 1*b*). The $H-K$ color behaves in an opposite manner (at first increasing in magnitude and then decreasing). It is perhaps surprising that the azimuthal colors should behave in similar manner for both the bright knotty outer ring and the diffuse inter-ring material. We will argue later than this is strong evidence that the inter-ring material and the outer ring share a common history.

The similarity in surface brightness between the inter-ring and outer ring regions provides additional evidence that these two regions share some common properties. Figure 6*a* plots the K-band surface brightness of the inter-ring region and the outer ring as a function of azimuth. Figure 6*b* shows an analogous diagram for the B-band surface brightness. The surface brightness profile for both regions shows a peak which is repeatable at both the near-IR and the optical wavelengths. The azimuthal shift between the peak in the inter-ring region and the outer ring will be discussed in § 4.3.

3.4. *Magnitudes and Colors of the Knots*

Table 3 lists the magnitudes and colors for the knots labeled in Figure 1*c*. These data have been corrected for Galactic extinction only. Figure 7*a* is a $B-V/V-K$ plot of the knots, and Figure 7*b* is a $J-H/H-K$ plot. (For comparison, the

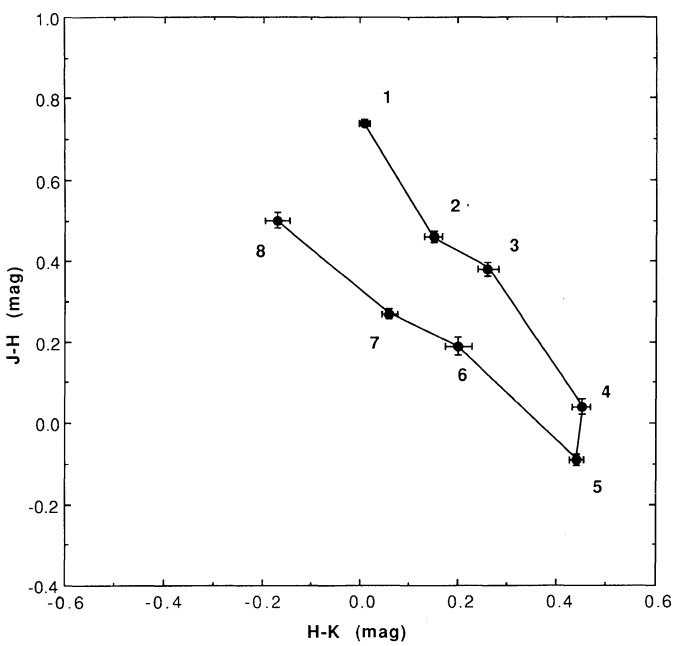

FIG. 5*a*

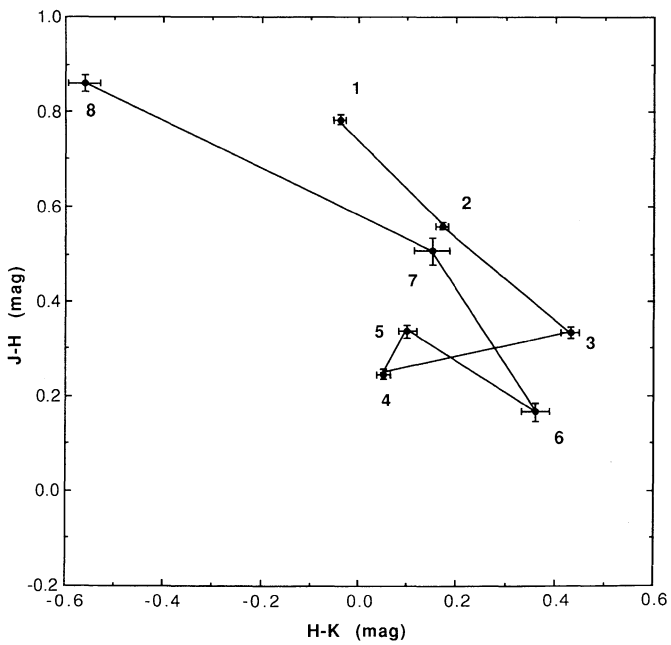

FIG. 5*b*

FIG. 5.—(*a*) The $J-H$, $H-K$ colors for each wedge as numbered in Fig. 1*b*. This demonstrates the azimuthal variations in the colors of the material between the inner and outer rings. The position angle is measured counterclockwide from wedge 1. (*b*) Same as (*a*), but for the outer ring only. Note the similarity between (*a*) and (*b*).

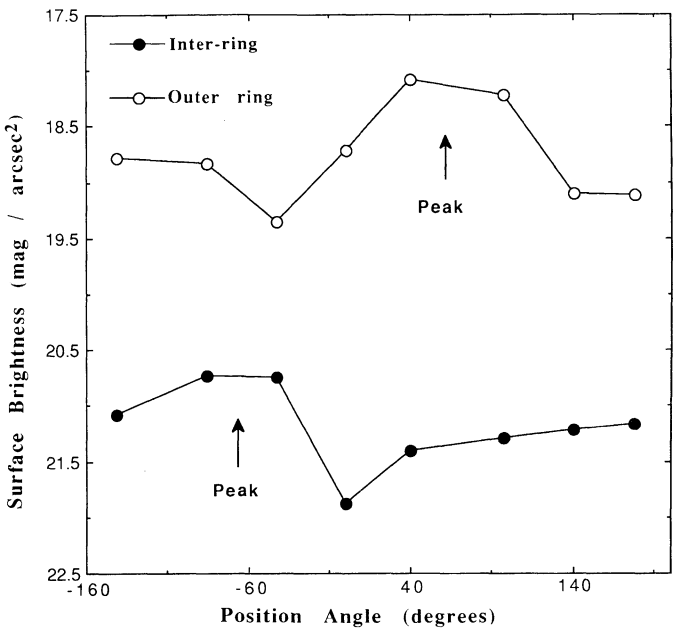

FIG. 6a

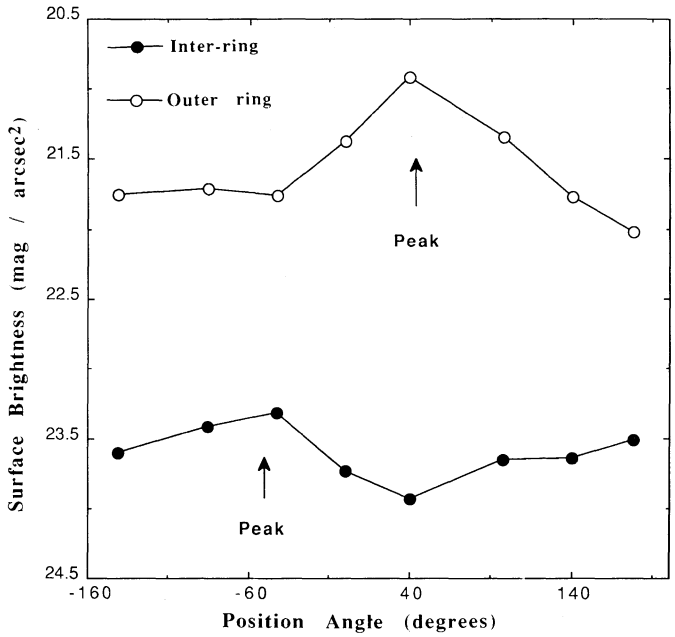

FIG. 6b

FIG. 6.—(*a*) The *K*-band surface brightness as a function of azimuth for the inter-ring (*filled circles*) and outer ring (*open circles*) regions. The wedge-shaped apertures in Fig. 1*b* were used for the calculation of these magnitudes. For clarity, the outer ring data have been shifted upward in the diagram by 2 mag arcsec^{-2}. (*b*) Same as (*a*), but for the *B*-band data. The outer ring data have been shifted upward in the diagram by 1 mag arcsec^{-2}.

azimuthally averaged radial colors for the entire Cartwheel, which were presented in Figures 3 and 4, are also shown in Figures 7*a* and 7*b*, respectively.) Based on their absence from images taken in Hα and λ-21 cm continuum emission (Higdon 1992), knots 6 and 9 are most likely foreground stars. As mentioned earlier, the internal extinction in the outer ring is very uncertain. Nevertheless, for purposes of the luminosity calculations, we have applied the FH value of $A_V = 2^{m}.1$ globally to all the knots (See Table 3).

4. CONFIRMATION OF A COLLISIONALLY GENERATED RING

4.1. *Morphological Predictions of the Model*

The ASM cloud-fluid models predicted that star formation would be nonlinearly suppressed immediately behind a strong

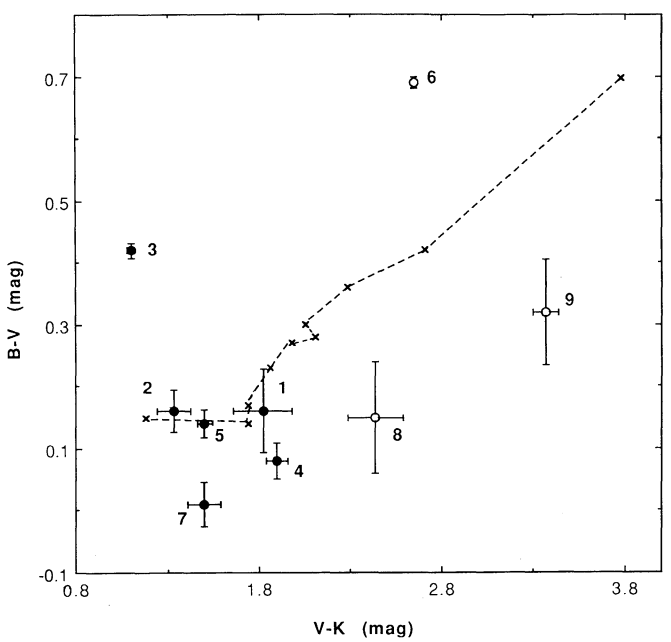

FIG. 7a

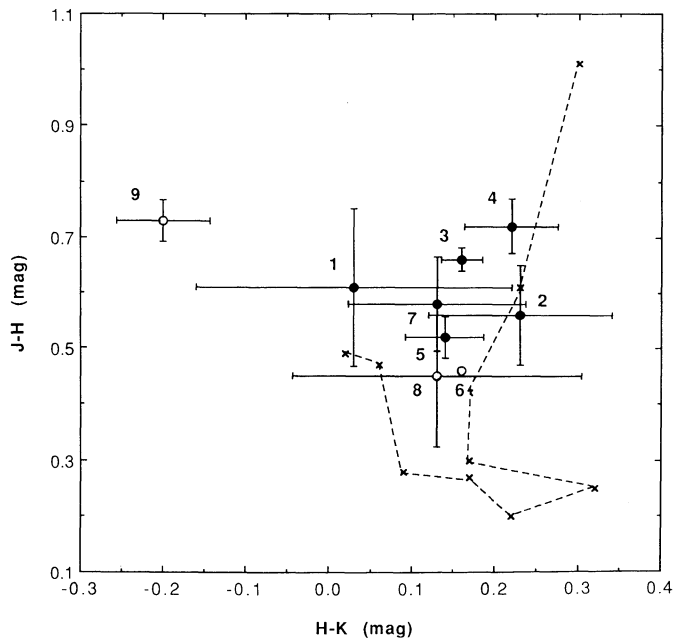

FIG. 7b

FIG. 7.—(*a*) $B-V/V-K$ plot, with 1 σ error bars, for the knots which are labeled in Fig. 1*c*. The azimuthally averaged colors (see Fig. 3) are overlaid for comparison. Solid circles represent data which are associated with the outer ring. Open circles are either knots located in the inter-ring region or are foreground stars. (*b*) $J-H/H-K$ plot for the same knots, with 1 σ error bars.

TABLE 3

OPTICAL AND NEAR-INFRARED PROPERTIES OF THE KNOTS[a]

Knot	J (mag)	B (mag)	$J-H$ (mag)	$H-K$ (mag)	$B-V$ (mag)	$V-K$ (mag)	L_B[b] (ergs s^{-1})	L_K[b] (ergs s^{-1})
1	18.43	19.80	0.61	0.03	0.16	1.82	5.5×10^{41}	2.3×10^{40}
2	17.93	18.66	0.56	0.23	0.16	1.33	1.6×10^{42}	4.1×10^{40}
3	16.35	17.08	0.66	0.16	0.42	1.10	6.7×10^{42}	1.8×10^{41}
4	17.34	18.41	0.72	0.22	0.08	1.90	2.0×10^{42}	8.2×10^{40}
5	16.90	17.91	0.52	0.14	0.14	1.50	3.1×10^{42}	9.5×10^{40}
6[c]	13.67	16.42	0.46	0.16	0.69	2.65	...	...
7	17.86	18.69	0.58	0.13	0.01	1.50	1.5×10^{42}	4.1×10^{40}
8	18.24	20.28	0.45	0.13	0.15	2.44	3.5×10^{41}	2.6×10^{40}
9[c]	17.04	20.23	0.73	−0.20	0.32	3.37	...	...
Outer ring[d]	13.70	14.72	0.50	0.06	0.15	1.41	7.4×10^{43}	1.6×10^{42}

[a] All magnitudes and colors corrected for Galactic extinction ($A_B = 0^m22$, RC2) only.
[b] An extinction of $A_V = 2^m1$ (FH) has been applied to all luminosity calculations (see text).
[c] Foreground stars.
[d] Calculations based on total integrated flux from the outer ring.

density wave. Additionally, the models predicted a similar rarefraction in the distribution of old stars. Such a "hole" is evident in the southern quadrant of all three near-IR images (see Figs. 1*a*–1*c*), as well as in the optical images (not shown here). Even after smoothing, there is no evidence of faint emission in this region in the K-band image (see Fig. 1*d*).

If the ring is defined by young stars, then the numerical models also predict the first (outer) ring to be "crisp" (ie., to have well-defined edges) as a result of the nonlinear enhancement of star formation. The smoothed K-band image (Fig. 1*d*) shows the outer ring to have a sharp edge with no emission exterior to it.

4.2. *Stellar Evolution behind the Ring*

As the density wave propagates outward, it is expected to induce star formation in the gas disk. The newly formed stars are left behind in the wake of the ring. Therefore, one consequence of the collisional model for ring galaxies is that of a time-lapse sequence of stellar evolution as a function of radius. We have already demonstrated that the galaxy displays an unusually large radial color gradient. We now wish to determine whether these gradients are what would be expected from the evolution of a starburst population formed in the ring. Assuming an oversimplified picture in which the ring expansion velocity is approximately constant, the outer ring represents the site of the most recent star clusters ($t = 0$) and each annulus within the ring corresponds linearly to some time since the burst.

Color predictions for the evolution of a starburst population have been the subject of much interest in recent years. Figures 8*a*–8*b* are $B-V/V-K$ diagrams presenting the evolutionary tracks from models by Charlott & Bruzual (1991, hereafter CB) and, for comparison, the older predictions of Struck-Marcell & Tinsley (1978, hereafter ST). The models of CB are for a young starburst population which has an initial short-lived star formation phase followed by an abrupt cessation of star formation. On the other hand, the models of ST are for a constant star formation rate. The "loop" to the red in the CB model corresponds to the red supergiant flash (RSG), which is a feature of more recent modeling of young clusters (Arimoto & Bica 1989). Also shown in Figures 8*a*–8*b* are the annular ring colors for the Cartwheel which were first presented in Figure 3. Figure 8*b* is an enlarged view of these data, showing the 3 σ error bars. Note how these points follow the models along the direction of increasing time in the order expected from the collisional model, i.e., bluest points in the outer ring (points 8 and 9), reddest points in the inner ring (point 1). The good correspondence between the models and the observations provides strong support for the collisional picture of the formation of the ring. The outer ring points lie in the region of the diagram corresponding to the youngest evolutionary stages of the starburst, while the inner regions lie in the part of the diagram corresponding to evolved stars. The radial expansion velocity of the ring was derived by FH to be 90 km s^{-1} and the radius of the ring is 17.3 kpc (for $D = 89$ Mpc). Therefore an approximate expansion time for the outer ring is of the order of 2×10^8 yr. Now, the reddest and innermost point in the inter-ring region is point 2 of Figure 8*b* which lies closest to the CB cluster evolution at the RGB phase, corresponding to a time of $\sim 4 \times 10^8$ yr. On the other hand, the corresponding age of a cluster of this color in the ST constant star formation model is ~ 4 Gyr. The correspondence between the dynamical time scale and the age of the density wave as predicted by the CB single-burst model is consistent with the hypothesis that we are observing the evolution of a starburst population formed in the wake of the expanding ring.

In the cloud-fluid models of ring galaxies, ASM and SMA predicted that the infall of gas behind the first ring should lead to a strong compression of gas in the second ring. Consequently, one should expect to see much star formation near the inner ring. However, both the lack of strong emission lines from the inner ring and the later-type colors of the inner ring suggest that the second ring is a density wave in a mainly old stellar population. The stars in the inner ring may represent the evolved starburst created during the early history of the first density wave. Taking the position of the inner ring in Figure 8 literally, the age of the stellar content of the inner ring is $\sim 6 \times 10^8$ yr, which is approximately consistent with the dynamical age of the first ring. On the other hand, the stars may be the remnants of a small stellar disk which existed before the collision. In any case, the suppression of star formation in the inner ring is most likely due to a lack of neutral gas in the inner regions. A possible explanation for this deficiency is that the central gas disk was stripped by the passage of the intruder galaxy through the nucleus. High-resolution VLA mapping of the region between the Cartwheel and one of its companion galaxies supports this view (Higdon 1992).

The nucleus has anomalous colors when compared with the

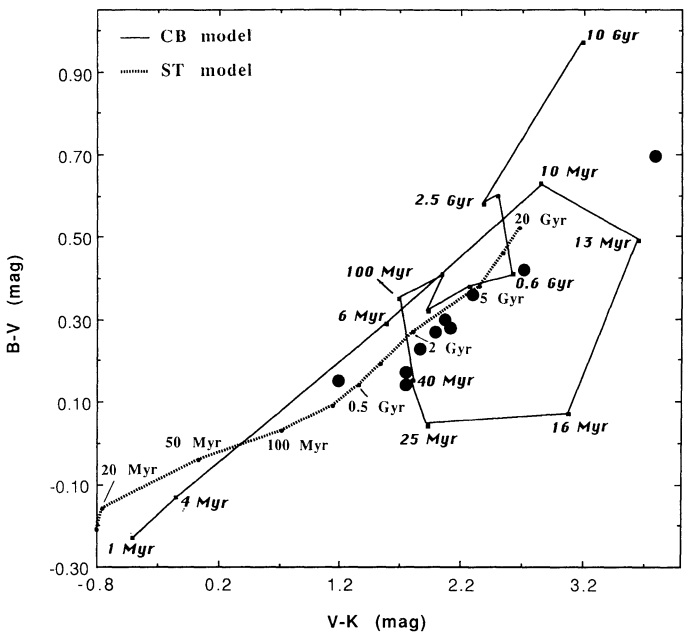

FIG. 8a

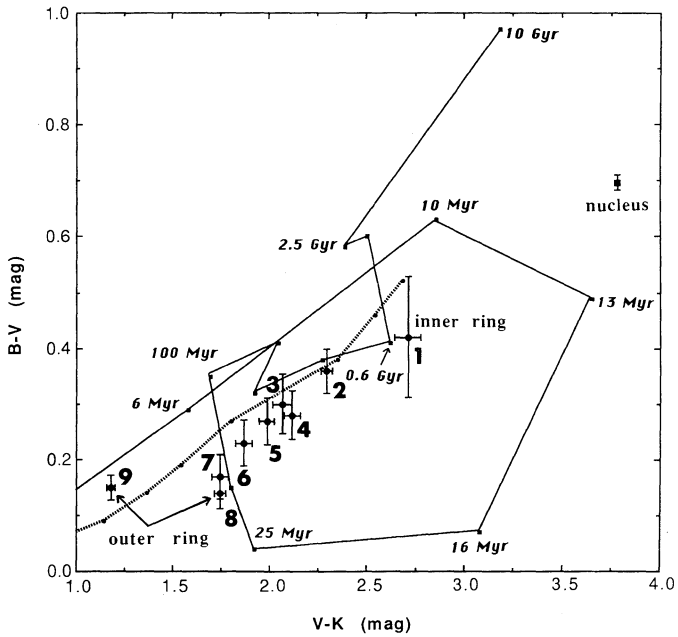

FIG. 8b

FIG. 8.—(*a*) The same data as given in Fig. 3, but superposed on the diagram are the ST (constant star formation; *dotted line*) and CB (single starburst, *solid line*) models for color evolution. (*b*) A close-up view of the data in (*a*). Point 1 is in the inner ring, point 8 is the inner edge of the outer ring, and point 9 is the outer edge of the outer ring. Error bars represent a 3 σ limit.

models. The nucleus of the Cartwheel lies too far to the red of either the starburst or the constant star formation rate models of cluster evolution. However, the old stellar content of the nucleus is confirmed by the detection of a late-type stellar absorption spectrum with Ca II H and K lines, the G band, and Mg I band (FH). The $J-H/H-K$ colors for the nucleus are consistent with those of an evolved population of M giants, thus the discrepancy between the $B-V/V-K$ colors and the models may relate to uncertainties in the models at late times, especially in the treatment of AGB and carbon-rich LPV stars.

The $J-H/H-K$ colors within the disk (see Fig. 4) are more difficult to interpret as evidence for an "age gradient" in the stellar population. One explanation for the cyclic behavior discussed in § 3.2 is the possible contribution of hot dust to the K-band emission. If the collisional picture is correct, a large population of stars will simultaneously go through the red-giant and AGB phases downstream of their formation site in the ring. If so, then large numbers of stars may develop circumstellar dust shells. Spectroscopic observations and longer wavelength IR observations will be required to investigate this idea.

Finally, we discuss the rather large $V-K$ color gradient seen in the outer ring. In Figure 3, the $V-K$ color becomes significantly larger across the outer ring ($0^m.6$ over $6'' = 3$ kpc). We have confirmed that the inner edge of the outer ring has a $V-K$ color that is significantly redder than its outer edge by carefully measuring colors in the highest signal-to-noise regions. The large gradient across the outer ring is also seen in the $H-K$ color (see Fig. 4). Because the seeing in the H band and the seeing in K band were virtually identical, the gradient cannot be attributed to the effects of variable seeing at different wavelengths. One way that this rather sharp gradient can be reconciled with the models is that the outer edge of the ring is so young that it has not yet produced any red supergiants, whereas the inner edge of the ring is in the post–red-flash stage; i.e., stars on the inner edge of the ring, point 8 of Figures 8*a*–8*b* are ~40 Myr older than stars on the outer edge, point 9. Given the lifetime of O/B stars, this is consistent with the expansion velocity of 90 km s^{-1} of FH and a ring thickness of 3 kpc. Given this explanation for the gradient in the outer ring, we should expect to see some regions of the ring caught in the red-flash stage. As the models of CB show, such regions would have large $V-K$ colors in the range $2^m.5$–$3^m.5$. However, the only knots which show $V-K$ colors this large are knots 6, 8, and 9, which are unassociated with the outer ring (see Fig. 7*a*). Because of the extremely rapid evolution along the red side of the RGB "loop" (only ~20 Myr), it is possible that we have not been fortunate enough to "catch" one of the knots in this stage of evolution.

4.3. *Azimuthal Color Gradients*

One of the perplexing aspects of the Cartwheel ring galaxy is the origin of the optical "spokes" which connect the inner ring to the outer ring. Our surface photometry has shown that at least one of the two main spokes (specifically, the east spoke) shows up quite clearly in the azimuthal surface brightness profiles at both optical and near-IR wavelengths (the "peak" in Figs. 6*a*–6*b*). The remarkable similarity between the shape of the azimuthal surface brightness profile for the inter-ring and that of the outer ring, and the similarity between the azimuthal color variations for these two regions, provide evidence that the inter-ring material is a faded relic of the outer ring. However, if the inter-ring material consists of stars evolving in the wake of the ring, then differential motion in the disk should have led to a phase difference between the inter-ring surface brightness profile and the outer ring. Indeed, there is a phase difference of ~120° between the profiles of Figure 6*a* and Figure 6*b*. This is in the sense that the outer ring features occur at a larger position angle than the inter-ring features. If the phase shift is a result of differential motion in the disk

(assuming that the direction of rotation is N–E), then $V_{rot}/V_{rad} = \Delta\theta\,(R_{out}/\Delta R) \sim 4$ (assuming that $R_{out}/\Delta R \sim 2$). This suggests a smaller expansion velocity (V_{rad}) for the ring than that measured by FH ($V_{rot}/V_{rad} = 254/89 = 2.9$). The smaller V_{rad} which we calculate, $254/4 = 64$ km s^{-1}, is in better agreement with recent H I measurements (Higdon 1992). FH suggested that the spokes are a result of differential rotation of original clumpiness within the disk. The striking similarity in the azimuthal color gradient and surface brightness of the inter-ring material and that of the outer ring strongly support this view and results from recent modeling by Struck-Marcell (1992). In these models, the clumpiness is enhanced by the passage of the ring, and are then sheared into spokelike structures.

5. CASE FOR AN INITIAL EPOCH OF STAR FORMATION WITHIN THE DISK

Previous studies have suggested that the Cartwheel galaxy is undergoing its first episode of disk-wide star formation. For example, spectroscopic studies by FH revealed a low metallicity; the oxygen, nitrogen, and neon are deficient by factors of 6 ± 2, 22 ± 4, and 3 ± 2, respectively as compared to solar values. The unusually low value for the nitrogen relative to oxygen is interesting, since it is believed that oxygen derives mainly from high-mass stars whereas nitrogen is produced in both high-mass and intermediate-mass stars (see Pagel 1981; Steigman, Gallagher, & Schramm 1989). These abundance measurements support the view that star formation is quite recent. Also, H I observations (Higdon 1992) indicate that a neutral gas disk extends beyond the outer ring, yet there is no evidence of a stellar population exterior to the outer ring in either the optical or near-IR images (see Figs. 1*a*–1*d*). Gas-rich, low surface brightness galaxies (Giovanelli & Haynes 1989; Brinks 1990; Impey & Bothun 1989; Schombert & Bothun 1988) could well be representative of the Cartwheel progenitor.

In the classical Toomre (1978) picture of the formation of a ring galaxy, the ring is a crowding of disk stars. Our original motivation in this study was to detect this wave and to measure its overdensity. However, all the evidence suggests that the ring is defined by newly formed stars. We find no evidence for the old stellar population. The numerical simulations predict that the density wave, composed of precollision stars, should be broader than the ring of star formation (e.g., ASM). The stellar component is predicted to have a FWHM which is at least twice as large as that of the star formation component. Because the outer ring is $\sim 6''$ in width, such an offset between these two rings would be resolvable in our images. Therefore, we should see a broad, smooth K-band ring and a narrower optical ring, since the K band traces the old stellar population. However, the FWHM has been measured at several positions along the outer ring in B and K, and no difference in FWHM is observed (see Fig. 2); the K-band emission seems to be coming from red supergiants (or heavily reddened O/B stars) rather than from an older generation of stars. An upper limit to the overdensity of any undetected underlying density wave is estimated to be $\Delta\rho/\rho < 0.2$. The lack of the underlying stellar ring suggests that there were little or no precollision disk stars in the Cartwheel progenitor before the collision.

Finally, the magnitude of the radial color gradient observed in the inter-ring material strongly suggests that the starlight is relatively uncontaminated by background light from a pre-existing stellar disk. Such a disk, if present, would presumably dilute any effects due to the formation of young stars and would tend to wash out large gradients. The similarity of the observed color gradients with the model-predicted colors of young star clusters argue that any such underlying disk must play little or no role in the observed colors of the inter-ring material and argues in favor of a pure gaseous disk at the time of the initial encounter.

6. PROPERTIES OF THE KNOTS

Both Figures 7*a* and 7*b* demonstrate that the dispersion of colors for the knots within the outer ring is small as compared to the color dispersion in the galaxy as a whole. What is immediately obvious from Figure 7*a* is that all of the outer ring knots (with the exception of knot 3) are bluer than the inter-ring region (points 1–7) in both $B-V$ and $V-K$. If one ignores the effects of internal extinction and takes the positions of the outer ring knots in the $B-V/V-K$ plot literally, then the ages of the knots range from 6 to 40 Myr (CB model). Unfortunately, the reddening vector is almost parallel to the evolutionary track and could bring the age of the points down to 4 Myr or less. Nevertheless, in any case the knots are definitely the youngest features within the galaxy.

Due to uncertainties in the amount of internal extinction, the infrared colors of the knots within the ring do not uniquely describe a pure stellar population (see Fig. 7*b*). Also, future infrared spectroscopic observations will be able to determine whether the colors are contaminated by molecular lines. Assuming emission line contamination is minimal, the colors could be interpreted as being dominated by (1) K and G main-sequence stars (assuming $A_v = 0^m$ for internal extinction), (2) heavily reddened OB stars (requiring $A_v \sim 5^m$), or (3) a mix of OB stars and supergiants, placing the knots somewhere in between these two extremes on the plot. Because there is no spectroscopic signature of evolved stars in the outer ring (FH), we reject (1) as a possibility. Although it is possible for large amounts of internal extinction to exist within the outer ring, the amount required by (2) exceeds that measured via optical (FH) data. Thus, we consider (3) to be most likely.

Assuming that a large fraction of the light at both the B and K bands comes from early-type stars, an order of magnitude estimate of the number of O stars present in the outer ring can be made. However, as argued above, the near-IR colors do not unambiguously prove that the outer ring is dominated by young stars and so our assumption must be born in mind when considering the results of the following analysis. An attempt to correct for internal extinction has been made by applying a global value of $A_v = 2^m.1$ (FH) in the calculation of the luminosities given in Table 3. We estimate the number of O5 V stars by assuming $M_v(O5) = -5^m.7$, $V-K = -0^m.94$ and $B-V = -0^m.32$ (Zombeck 1990). Thus $L_B(O5) = 2.0 \times 10^{37}$ ergs s^{-1} and $L_K(O5) = 2.4 \times 10^{35}$ ergs s^{-1}. With these assumptions, the total number of O5 stars contained within the outer ring is $5 \times 10^6\ h^{-2}$ and $7 \times 10^6\ h^{-2}$ for the B and K bands, respectively. For comparison, $N(O6) = 1 \times 10^5\ h^{-2}$ and $N(O5) = 5 \times 10^5\ h^{-2}$, from the H$\beta$ luminosity and integrated optical continuum, respectively (FH). An independent upper limit to the total number of OB stars was obtained from the failure to detect the galaxy at X-ray wavelengths. The *Einstein Observatory* Imaging Proportional Counter (IPC) yielded an upper limit to the X-ray luminosity of $\log(L_x) < 42.5 \pm 0.9$ (Ghigo, Wardle, & Cohen 1983). Assuming that the dominant

X-ray flux would be from the corona of OB stars ($L_x = 10^{33}$ ergs s^{-1}), the upper limit corresponds to a total $8 \times 10^8\ h^{-2}$ OB stars contained within the entire galaxy.

The close agreement between N_K and N_B helps to substantiate the claim that the outer ring luminosity is dominated by young stars. Also, the close spatial correlation between the knots in both the B and K images supports the idea that the K light in the outer ring is tracing the young rather than old stars. The FH values for Hβ luminosity and integrated optical continuum were not corrected for internal extinction, and this is probably the reason that the FH values for N(O star) are a magnitude lower than those given by the B and K luminosities.

7. COMPANION GALAXIES

The companion galaxy which is responsible for the collision with the Cartwheel has not been identified, although one (or more) of the three closest northern galaxies (see Davies & Morton 1982) are the obvious candidates. Of the three, only galaxies 3 and 4 have near-IR colors suggestive of recent star formation. Neglecting internal reddening, the colors of galaxy 3 could be taken as those of supergiants. However, a modest amount of internal reddening ($A_v \approx 0^m.8$) could lead to a predominantly K dwarf population. The blue $J-H$, yet red $H-K$, colors of galaxy 4 could indicate a heavily reddened OB population (requiring $A_v \approx 6^m$). The colors of galaxy 2 are those of M dwarfs. The reddening vector is incapable of correcting the colors of galaxy 2 to the O/B region of the near-IR color-color plot (for reference, see Fig. 4.

8. CONCLUSION

Optical and near-infrared data ($BVJHK$) have been presented which provide evidence that the rings within the Cartwheel ring galaxy were created as a result of a collision with a companion galaxy. When compared to color evolution models, the azimuthally-averaged $B-V/V-K$ colors confirm that the stars are youngest in the outer ring and get older as one progresses inwards. Based on dynamical time-scale arguments, the CB model for a single starburst seems to fit the data better than the ST model for continuous star formation. Both the $J-H/H-K$ and $B-V/V-K$ colors suggest that the leading edge of the outer ring is the current site of star formation, as predicted by the ASM models. These models also predict that the rarefraction just behind the outer ring leads to a strong suppression of star formation there. A depression immediately behind the ring is observed in both the optical and near-IR images, indicating not only a suppression of star formation, but also a lack of underlying precollision stars.

Our data support results from spectroscopic and H I measurements that the galaxy is undergoing its first epoch of star formation within the disk. The lack of optical or near-infrared emission outside of the outer ring implies that the outer ring is generating a burst of star formation within a primordial or low surface brightness H I disk. Also, radial color gradients ($J-H$, $H-K$, $B-V$, $V-K$) which are ~ 8 times greater than typical values for disk galaxies, are observed within the disk of the Cartwheel. Such strong gradients would not be expected if there were an underlying evolved stellar disk. Finally, we find no evidence for a ring consisting of old disk stars. All the evidence suggests that the density wave generated by the collision is driven into a predominantly gaseous disk.

The azimuthal behavior of the colors and surface brightness profiles in the inter-ring regions are very similar to that of the outer ring. A peak in the K and B surface brightness profiles is seen in both of these regions. A phase shift in the azimuthal position of this peak between the two regions suggests an expansion velocity which is consistent with the value obtained from kinematic data. This result suggests that the "spokes" which are seen in the disk are related to a fading of ring knots which persist in the expanding ring.

It is a pleasure to thank Colin Aspin for his assistance with data acquisition and reduction during our stay at the UKIRT facilities. The many fruitful discussions with Curt Struck-Marcell are greatly appreciated. P. M. M. gratefully acknowledges the Iowa Space Grant College Consortium for the award of a NASA fellowship which provided both research and travel support. P. N. A. wishes to thank the Department of Physics and Astronomy at ISU for travel support.

REFERENCES

Appleton, P. N., & Struck-Marcell, C. 1987, ApJ, 318, 103 (ASM)
Arimoto, N., & Bica, E. 1989, A&A, 222, 89
Bessell, M. S., & Brett, J. M. 1988, PASP, 100, 1134
Brinks, E. 1990, in Dynamics and Interactions of Galaxies, ed. R. Wielen (Berlin: Springer), 146
Charlott, S., & Bruzual, A. 1991, ApJ, 367, 126 (CB)
Christian, C. A., Adams, M., Barnes, J. V., Butcher, H., Hayes, D. S., Mould, J. R., & Siegel, M. 1985, PASP, 97, 363
Davies, R. L., & Morton, D. C. 1982, MNRAS, 201, 69p
de Vaucouleurs, G., de Vaucouleurs, A., & Corwin, Jr., H. G. 1976, Second Reference Catalogue of Bright Galaxies (Austin: Univ. of Texas Press) (RC2)
Fosbury, R. A. E., & Hawarden, T. G. 1977, MNRAS, 178, 473 (FH)
Ghigo, F. D., Wardle, J. F. C., & Cohen, N. L. 1983, AJ, 88, 1587
Giovanelli, R., & Haynes, M. P. 1989, AJ, 90, 2445
Griersmith, D., Hyland, A. R., & Jones, T. J. 1982, AJ, 87, 1106
Higdon, J. L. 1992, in preparation
Impey, C., & Bothum, G. 1989, ApJ, 341, 89
Lynds, R., & Toomre, A. 1976, ApJ, 209, 382
Pagel, B. E. J. 1981, in The Structure and Evolution of Normal Galaxies, ed S. M. Fall & D. Lynden-Bell (Cambridge Univ. Press), 211
Schombert, J. M., & Bothum, G. D. 1988, AJ, 95, 1389
Schultz, A. B., Spight, L. D., Colegrove, P. T., DiSanti, M. A., & Fink, U. 1990, in ASP Conf. Ser., Vol. 10, Proc. Edwin Hubble Centennial Symp., Evolution of the Universe of Galaxies, ed. R. G. Kron (San Francisco: ASP), 182
Spight, L. D., Schultz, A. B., Colegrove, P. T., DiSanti, M. A., & Fink, U. 1990, in ASP Conf. Ser., Vol. 10, Proc. Edwin Hubble Centennial Symp. Evolution of the Universe of Galaxies, ed. R. G. Kron (San Francisco: ASP), 179
Steigman, G., Gallagher, J., & Schramm, D. N. 1989, Comm. Astrophys., 14, 97
Struck-Marcell, C. 1992, preprint
Struck-Marcell, C., & Appleton, P. N. 1987, ApJ, 323, 480 (SMA)
Struck-Marcell, C., & Tinsley, B. M. 1978, ApJ, 221, 562 (ST)
Theys, J. C., & Spiegel, E. A. 1976, ApJ, 208, 650
———. 1977, ApJ, 212, 616
Thompson, L. A., & Theys, J. C. 1978, ApJ, 224, 796
Toomre, A. 1978, in IAU Symp. 79, ed. M. S. Longair & J. Einasto (Dordrecht: Reidel), 109
Zombeck, M. V. 1990, Handbook of Space Astronomy and Astrophysics (Cambridge Univ. Press), 68, 71